Egypt. J. Chem. **Vol. 63**, No. 10. pp. 4107 - 4117 (2020)

Egyptian Journal of Chemistry

http://ejchem.journals.ekb.eg/

Modeling and Optimization of Synthesis Condition of $CuCr_2O_4$ Spinel for CO Oxidation

Mahnaz Yasemi[a],*, Ali Tarjomannejad[b]

[a]*Department of Chemical Engineering, Eyvan-e-Gharb Branch, Islamic Azad University, Eyvan-e-Gharb, Iran*

[b]*Department of chemical engineering & petroleum, University of Tabriz, Tabriz, Iran*

Abstract

In this paper, the $CuCr_2O_4$ spinel catalyst was synthesized by the Pechini method, and its activity was evaluated in catalytic oxidation of CO. $CuCr_2O_4$ spinel catalyst was characterized by XRD, BET, H2-TPR, and SEM. This catalyst has a good ability in CO oxidation. The effects of three synthesis variables (EG/citrate, citrate/nitrate ratio, and calcination temperature) and reaction temperature as an operational variable on CO conversion were investigated. Based on the results, the optimum neural network architecture succeeded to predict CO conversion data with an acceptable level of accuracy. The model predicted that the relative importance of variables is as follows: calcination temperature > citrate/nitrate ratio > EG/citrate ratio. The optimum neural network architecture was used as a fitness function for the genetic algorithm to find the optimum catalyst. Under the optimum condition (EG/citrate: 3.24, citrate/nitrate ratio: 0.62 and calcination temperature: 620 °C), the predicted optimum value of CO conversion was found to be in a good agreement with the corresponding actual value.

Keywords: CO oxidation; CuCr2O4; Spinel; Catalyst design; Artificial Neural Network

1. Introduction

Carbon monoxide is one of the main gaseous pollutants, which is generally released from the combustion of fossil fuel in diesel engines [1]. There are many methods for removal of CO including adsorption, thermal elimination, and catalytic oxidation. Catalytic oxidation of CO is proved to be one of the most efficient techniques to remove this pollutant [2, 3]. Present catalysts are supported noble metal catalysts based on platinum, palladium, and rhodium [4, 5]. High cost, low stability, and lack of noble metal limit their applications. Spinel-type oxides are interesting catalysts for CO oxidation. They have lower cost and higher thermal stability than supported noble catalysts [6, 7].

Some types of catalysts in chemistry have a special structure. Spinel metal oxides are one of them which have attracted much attention for their remarkable catalytic properties, for example in catalytic combustion of volatile organic compounds. The compositions of spinel catalysts are interdependent and the total mole fraction is considered one. The composition and metal type used in spinel catalysts affect the structure and activity of the catalyst. On the other hand, the synthesis process of these catalysts is usually difficult. When using traditional methods, it is difficult to determine the combined influences of each component the composite on the activity of catalysts, particularly interaction them effect. Statistical strategies can provide facile and effective approaches to establish a quantitative relationship between dependent and independent variables [8].

There are some papers about the application of spinel-type oxides in CO oxidation. $CuCr_2O_4$, $CuCo_2O_4$, and $CoCr_2O_4$ spinels were found to be very active for CO and hydrocarbons oxidation, as well as for catalytic removal of NOx and diesel soot [9-15]. It has been proven that mixed oxides exhibit improved property rather than individual oxides, especially in

*Corresponding author e-mail: mahnazyasemi@yahoo.com
Revised 03/08/2020; Accepted 10/10/2020
DOI: 10.21608/EJCHEM.2020.28417.2609

environmental catalysis. These metals are environmentally friendly [16-19]. Catalyst design is a complex process involving many steps and variables as well as complex interactions among these variables, which make the experimental studies quite expensive and time-consuming [20, 21]. With the advancements in the scope of information technology, catalysts design by computer is very important [22, 23]. Compared to traditional approaches, catalyst design not only can come to better catalyst design by a few experiments within a short period, it eliminates the need for knowing catalytic mechanisms completely. Regarding artificial neural networks (ANNs) capabilities in terms of function approximation and genetic algorithm (GA) capabilities in terms of searching the complex spaces, combined ANN-GA approaches can be used to model and optimize catalyst activity [24]. Hou et al [21] developed an ANN (called BP network) to design a VSbWSn (P, K, Cr, Mo)/SIAL catalyst for propane ammoxidation. Huang et al. [24] used a back-propagation network along with the Levenberg–Marquardt training method to simulate the relations between components of the catalyst, C2 selectivity, and methane conversion. In other work, they used a hybrid ANN-based GA to design a catalyst for the oxidative coupling of methane [25]. They succeeded to enhance methane conversion and C2 hydrocarbons selectivity. They showed that the proposed catalyst design approach was highly efficient and universal. Valero et al. [22] combined neural networks and GA to optimize the discovery of new materials and process conditions in catalytic reactors at an industrial scale. Zonouz et al. [26] used neural networks and GA to optimize the toluene oxidation activities of sol-gel synthesized $La_{1-x}Ce_xMn_{1-y}Cu_yO_3$ perovskite-type catalysts. In other work, Soleimanzadeh et al. [27] employed two statistical methods including the response surface method (RSM) and artificial neural network, for modeling and optimization of selective catalytic reduction of NOx with NH_3 (NH_3-SCR) over V_2O_5/TiO_2 nanocatalysts. In these two works, the authors successfully optimized the catalysts.

The aim of this work is modeling and optimization of preparation conditions of CuCr2O4 obtained by the Pechini method for catalytic oxidation of CO. Four factors, namely EG/citrate, citrate/nitrate ratio, and calcination temperature and reaction temperature were modeled simultaneously using an ANN. The obtained optimum structure of ANN was used as a fitness function for hybrid GA to find the optimum catalyst.

2. Experimental Section

2.1. Catalyst preparation

$Cu(NO_3)_2{\cdot}3H_2O$, $Cr(NO_3)_3.9H_2O$, Citric acid monohydrate, and Ethylene Glycol (EG) were purchased from Sigma-Aldrich company. Catalysts were prepared using the Pechini method. Stoichiometric amounts of $Cu(NO_3)_2.3H_2O$ and $Cr(NO_3)_3.9H_2O$ with a mole ratio of 1:2 were dissolved in a minimum amount of distilled water (50 ml of distilled water). Citric acid and ethylene glycol were used as the monomers for the formation of the polymeric matrix. Ethylene glycol and citric acid in the molar ratio of 4:1 were added to metal nitrates solution. Three major reactions: chelation, esterification, and polymerization successively occurred and black polymeric precursor was formed. The resulting mixture is heated to 80°C; was evaporated the water and forms a gel. Then the gel was burned at 200 °C and turned into a dark powder. The powder was calcined at 700 °C for 5 h [13].

2.2. Catalyst characterization

Identification of crystalline phases carried out using X-ray diffraction (XRD) on a SIEMENS D500 diffract meter (Germany) and Cu Kα radiation (λ = 1.54 A). Diffract grams were recorded with a step of 0.25˚ per minute for 2θ between 10 and 90˚. The BET surface area was estimated by N_2 adsorption-desorption porosimetry at 77 K using an Autosorb-1 Quantachrome analyzer. Infrared (IR) spectra were recorded with a Bruker 27 FT-IR spectrometer using the Universal ATR Accessory in the range from 4000 to 400 cm^{-1} with a 4 cm^{-1} resolution. The temperature-programmed reduction (TPR) experiment was carried out in a Micrometritics Autochem 2900. The H_2-TPR experiment was performed with a 5% H_2/Ar gas flow at 20 standard cubic centimeters per minute (SCCM) and a linear heating rate of 10 ºC/min at 50-700 ºC. The morphology of the spinel catalyst was determined via scanning electron microscopy (SEM) by TESCAN (Czech Republic) instrument.

2.3. Catalytic activity

The activities of catalyst in CO oxidation were tested in a conventional fixed bed reactor (l = 50 cm, i.d. = 1 cm) under atmospheric pressure and at different temperatures between 50-300 °C. An amount of 500 mg of catalyst was placed between two quartz wool plugs. The total flow rate of feed was 200 cm^3min^{-1}. Feed composed of 2% CO, 20% O_2, and Ar. The feed and gas product analyzed using a Varian 3400 equipped with a TCD detector and a molecular sieve 13X (Supelco) packed column. Before the data were obtained, reactions were maintained for some time at each temperature to ensure steady-state conditions. The conversion efficiency was calculated by equation 1.

$$CO\ Conversion\ (\%) = \frac{CO_{in} - CO_{out}}{CO_{in}} \times 100 \qquad (1)$$

3. Computational Details

3.1. Design of experiments

In this study, the effects of the EG/citrate, citrate/nitrate ratio, and calcination temperature on the conversion of CO (response) were studied. Central composite design (CCD) was employed to design the experiments. For each factor, 5 levels were defined. These values were designated by the codes –1.6, –1, 0, +1, and +1.6 and are given in table 1. The ranges of the independent variables were determined by considering the literature. A total of 20 experiments were designed using CCD. The designed experiment included six replicates at the central point, six ones at axial points, and eight ones at factorial points.

Table 1

The levels of the independent variables in actual and coded value

parameter	Level				
	-1.681	-1	0	1	1.681
EG / Citric acid	2	2.8	4	5.2	6
Citric acid / total nitrate	0.2	0.32	0.50	0.68	0.8
Calcination Temperature (°C)	600	640	700	760	800

3.2. Artificial neural network

Artificial neural networks are used in a broad range of applications such as the prediction of thermodynamic properties. ANNs usually consist of an input layer, an output layer, and one or more hidden layers [28]. The number of neurons in the input and output layer depends on the respective number of dependent and independent parameters [29]. Dependent and independent parameters are considered as input and output parameters, respectively. The output of each neuron is calculated by equation 2 [30].

$$y_j^h = g\left(\sum_i^n w_{ij}^h\, y_i^h + b_j^h\right) \qquad (2)$$

Where y_j^h the output of the jth neuron is, w_{ij}^h is weight connecting *i*th neuron (from the previous layer) to *j*th neuron in the current layer, y_i^h is the output of *the i*th neuron, b_j^h is a bias of *j*th neuron and g is a transformation function. The transformation functions are usually hyperbolic tangent sigmoid (tansig) and linear (purelin) which are defined in equations 3 and 4, respectively [31]:

$$y_j = \frac{1}{1 + e^{-S_j}} \qquad (3)$$

$$y_j = S_j \qquad (4)$$

One of the reasons for using these transformation functions is the ease of evaluating the derivatives for minimization of the error function. The experimental data were divided into three sets including training, validation, and testing data sets. The training data set was used to optimize the weights and biases of the network to minimize the error between experimental and predicted data while testing the data set was used to examine the ability of the network to predict the data that not used in the training process. The difference between experimental and testing data can show the ability and accuracy of the trained neural network.

The selection of a training algorithm is a critical step in neural network modeling [31]. Several training algorithms exist for optimization of weights and biases such as back propagation, gauss-newton, and gradient descent, but the back-propagation method usually has better results in the prediction of material properties. The number of neurons in the hidden layer has a significant role in the prediction ability of the network [30]. If an ANN has too few neurons, it may not have enough degrees of freedom to precisely approximate the desired function. If an ANN has too many neurons, it will learn the exemplars perfectly, but its additional degrees of freedom may cause it to show implausible behavior for untrained inputs; it then presents the poor ability of generalization. Since no information about the optimal number of neurons has been reported for the calculation of saturated properties, trial and error

is the best way to determination the optimal number of neurons.

To examine the efficiency and accuracy of the proposed ANN model for the prediction of saturated properties of refrigerants, some statistical parameters including root mean square error (RMSE) and correlation coefficient (R^2) was utilized which represented in equations 5 and 6 [31].

$$RMSE = \sqrt{\frac{1}{N}\sum_{i=1}^{N}\left(A_i^{exp} - A_i^{cal}\right)^2} \quad (5)$$

$$R^2 = \frac{\sum_{i=1}^{N}\left(A_i^{exp} - \bar{A}\right)^2 - \sum_{i=1}^{N}\left(A_i^{exp} - A_i^{cal}\right)^2}{\sum_{i=1}^{N}\left(A_i^{exp} - \bar{A}\right)^2} \quad (6)$$

Where $A_i^{\exp}$ is the ith experimental value, A_i^{cal} is the ith predicted value with ANN model, $\overline{A}$ is the average value of experimental data and N is the number of experimental data points. In terms of RMSE, the lower the better. R^2 explains to what extent the variance of one variable explains the variance of the second variable. So, if the R^2 of a model is 0.50, then approximately half of the observed variation can be explained by the model's inputs.

The relative importance of the input variables on the output can be evaluated using neural network weights according to equation 7.

$$I_j = \frac{\sum_j^n\left(w_{sj}u_{jk}/\sum_i^m w_{ij}\right)}{\sum_i^m\sum_j^n\left(w_{ij}u_{jk}/\sum_i^m w_{ij}\right)} \quad (7)$$

where I_j is the effect of jth input factor, wij is the weight that links the ith input to the jth neuron of the hidden layer, ujk is the weight which attaches jth neuron of hidden layer to kth output neuron, m is the number of input neurons (number of variables), n is the number of hidden layer neurons, and k is the number of outputs of the network which equals to 1 in the present work.

3.3. Genetic algorithm

In the proposed method, after developing the ANN model, a genetic algorithm (GA) was used to optimize input variables, to achieve maximum CO conversion. Each chromosome in the GA included three genes indicating three variables, namely Co mole fraction, the ratio of citric acid to total nitrate, and calcination temperature. All optimization calculations were done using MATLAB ™ genetic algorithm function in the command line. The selected parameters for the GA function are shown in Table 2. Figure 1 presents the methodology used in this paper at a glance.

Table 2

Selected parameters for genetic algorithm function

Property	Value or type	Property	Value or type
Population type	Double vector	Mutation function	Constraint dependent
Crossover fraction	0.8	Selection function	Stochastic uniform
Fitness scaling	Rank	Crossover function	Scattered

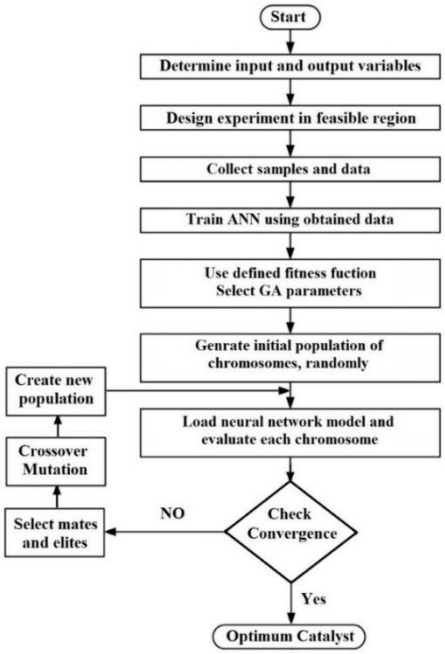

Fig. 1. Flow chart of optimization approach in this work

4. Results & Discussion

4.1. Characterizations

Figure 2 shows the XRD patterns of the $CuCr_2O_4$ spinel catalyst. A comparison of the XRD pattern with the standard card of $CuCr_2O_4$ (JCPDS 35-1321) confirmed the formation of spinel structure. No additional peaks were corresponding to the secondary phase or initial materials in the catalyst XRD pattern, which show metals are completely dissolved in the spinel structure. Figure 3 shows the XRD patterns for some of synthesized catalysts. As it clear in Figure 3, all of catalysts were synthesized in spinel structure.

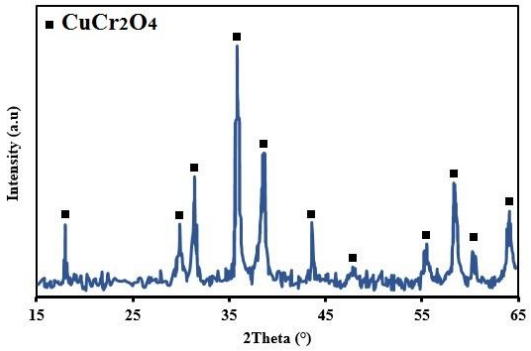

Fig. 2. XRD pattern of $CuCr_2O_4$ spinel

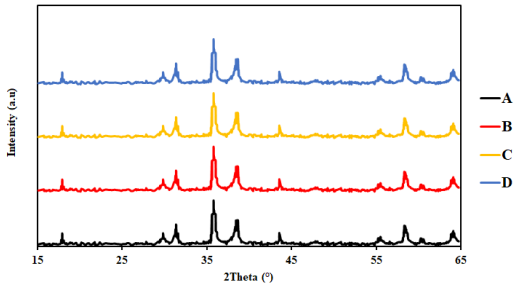

Fig. 3. XRD pattern of $CuCr_2O_4$ spinel: A) EG/CA=4, CA/TA=0.4, Tc=700 °C, B) EG/CA=2, CA/TA=0.4, Tc=600 °C, C) EG/CA=4, CA/TA=0.2, Tc=700 °C, D) EG/CA=4, CA/TA=0.8, Tc=700 °C

The infrared spectra in the range 400–3600 cm^{-1} of the synthesized spinel are presented in Figure 4. It can be seen that few organic groups are present in the synthesized spinel catalyst. The band at 3440 cm^{-1} is assigned to O-H stretching vibration [32]. The band around 1560 cm^{-1} is assigned to C=O stretching in carboxyl or amide groups. These bonds can also be related to the adsorption of carbon dioxide on the surface of samples [33].

The spinel-type oxide was shown two bands in the 700–400 cm^{-1} region, that it is the stretching vibration of the metal-oxygen bond. [34]. The band around 500 cm^{-1} is assigned to the vibration of Cu in the tetrahedral environment of the oxygen atom (Cu–O) and the band above 600cm^{-1} corresponds to the vibration of Cr in the octahedral (Oh) site of spinel. The appearance of these bands confirmed the formation of spinel structures. The bands around 615, 611, and 621 cm^{-1} correspond to bending modes of vibration of Cr–O in the Oh sites of spinel.

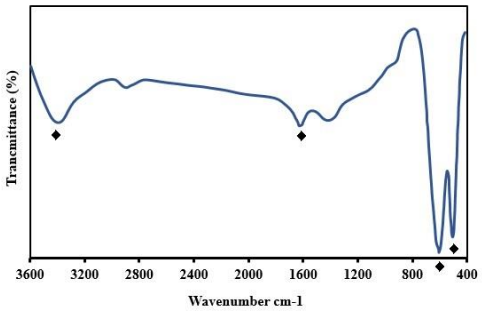

Fig. 4. FT-IR profile of $CuCr_2O_4$ spinel

The reduced ability of the spinel catalyst was investigated by the H_2-TPR experiment. H_2-TPR curve of the spinel sample is shown in Figure 5. The first reduction peak centered around 160 °C which could be attributed to the reduction of small and highly dispersed CuO particles and a second peak at 245 °C originated from the reduction of surface CrO_3 particles [35, 36]. Indeed, it is often reported in the literature that a fraction of the exposed Cr^{3+} ion in chromium oxide becomes readily oxidized to Cr^{6+} along the calcination step in the ambient atmosphere [37]. Above 400 °C, there is a main reduction consumption which is attributed to the reduction of bulk Cu^{2+} ions of $CuCr_2O_4$ to $CuCrO_2$, and the mixed oxide toward Cu^0 and Cr_2O_3 [35, 38].

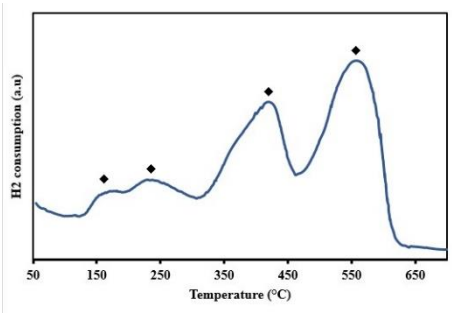

Fig. 5. H_2-TPR profile of $CuCr_2O_4$ spinel

The specific surface area of catalyst analyzed by the BET method and the surface area of $CuCr_2O_4$ is 12.2 m^2/g. Synthesis conditions can affect the specific surface area [39]. The specific surface area does not significantly affect the catalytic activity of the spinel catalyst for oxidation. Morphology of spinel catalyst was studied by SEM. The result from SEM (Figure 6) shows that the morphology of catalyst is irregularly shaped grains. As can be seen, the particle size

distribution is almost the same and its size is smaller than 100 nanometers.

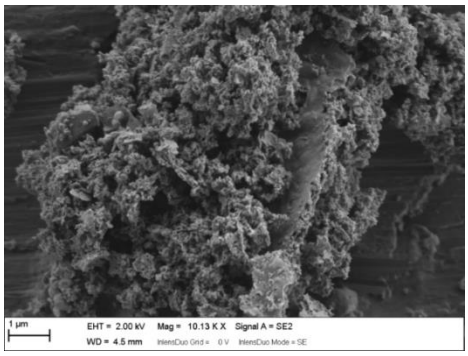

Fig. 6. SEM image of $CuCr_2O_4$ spinel

4.2. *Catalytic* activity

The temperature chart for CO conversions over the $CuCr_2O_4$ spinel is shown in Figure 7. CO conversion increases with temperature. $CuCr_2O_4$ spinel catalyst showed high activity in the range of 50–200 ºC. 90% CO conversion is achieved only at 170 °C.

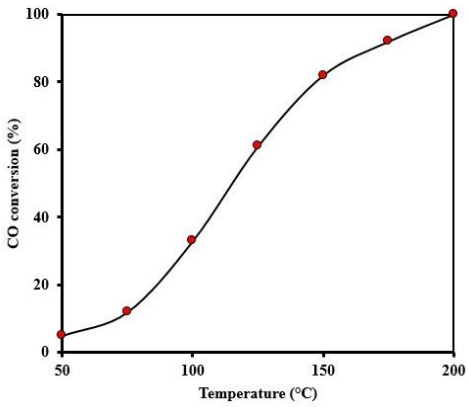

Fig. 7. The temperature profile of CO conversion over $CuCr_2O_4$ spinel

5. ANN modeling & validation

5.1. Topology Selection

The first step in the course of neural network modeling is to develop a database to train the network. Required database for training the neural network was obtained from experimental design at different temperatures. For modeling purposes, average CO conversion over repeated central points was used. A set of 90 experimental data points was used to develop the neural network model. Table 3 provides a summary of the matrix of experiments with the experimental results for CO conversion.

The next step is to declare input variables. Corresponding input variables to CO conversion estimation included the ratio of citric acid to total nitrate, the ratio of ethylene glycol to citric acid and calcination temperature, representing catalyst preparation parameters, and the reaction temperature, as an operational variable. Then, one should proceed to determine optimum topology.

The collected dataset was divided into three subsets, namely training, validation, and testing subsets, to not only find the optimum topology of the ANN model but have it evaluated in terms of correlative capability. The network randomly divides 70% of the data as training data, assigning 15% to the validation category and the remaining 15% to the test category. Figure 8 demonstrates the values of RMSE versus different numbers of neurons in hidden layers, for the training and testing data sets. The right side of Figure 8 magnifies the points around the optimal point. RSME in train, validation and test sets should be as close together as possible. Figure 8 shows that these values are well close together. As the figure shows, the network with 7 neurons in its hidden layer exhibited the least error, thus the best topology is the network with 7 neurons in hidden layer.

5.2. Model validation

After using the training data to model the catalyst performance, the k-Fold cross-validation method was employed for the generalization test of the achieved model. This method was implemented as follows: 15% of whole data was considered as test data. Data were divided into 10 sectors, and for each sector, 14 data were randomly selected as test data. Figure 9 shows RMSE values for training and testing for various categories together with their average. A low difference was observed in RMSE values, which confirmed a good generalization of the network. The proposed neural network model has 4 input layers, 7 hidden layers and one output layer is shown in Figure 10.

Table 3

CCD experiment matrix, experimental and ANN predicted values

No.	Variable			NO conversion											
				50 °C		75 °C		100 °C		125 °C		150 °C		175 °C	
	EG/CA	CA/TN	T Cal (°C)	Exp.	Pred.	Exp.	Pred.	Exp.	Pred.	Exp.	Pred.	Exp.	Pred.	Exp.	Pred.
1	2	0.50	700	4.3	0	10.9	9.4	29.0	31.7	56.3	58.4	76.7	77.8	88.8	86.9
2	2.8	0.68	640	9.9	2.0	17.0	15.7	41.6	39.2	70.2	65.2	89.0	83.2	97.4	92.2
3	4	0.20	700	4.6	5.4	10.9	12.5	26.6	27.6	48.0	51.0	69.1	73.1	87.2	86.3
4	4	0.50	700	6.9	6.8	12.7	16.2	34.3	35.1	62.9	61.1	83.8	82.8	93.1	94.6
5	2.8	0.68	760	7.2	4.1	14.6	15.5	38.9	36.9	66.9	63.1	87.3	82.7	94.0	92.7
6	5.2	0.68	640	3.2	2.7	11.4	12.7	32.5	32.4	58.0	57.4	78.5	76.9	89.9	87.7
7	4	0.50	700	8.3	6.8	13.8	16.2	33.6	35.1	63.1	61.1	82.9	82.8	93.5	94.6
8	6	0.50	700	0	0	9.3	6.4	23.7	22.0	45.1	46.1	62.3	68.8	84.2	82.8
9	4	0.50	700	7.8	6.8	14.1	16.2	34.8	35.1	63.7	61.1	82.0	82.8	93.7	94.6
10	4	0.50	700	9.2	6.8	13.7	16.2	35.8	35.1	62.1	61.1	83.5	82.8	94.5	94.6
11	4	0.80	700	3.7	2.6	10.7	14.4	31.2	36.0	58.5	61.7	78.4	80.4	88.2	90.3
12	4	0.50	600	7.6	7.6	15.4	18.4	38.8	39.1	65.4	65.1	86.9	85.3	94.7	95.9
13	4	0.50	700	9.0	6.8	13.9	16.2	35.1	35.2	61.8	61.1	83.1	82.8	93.8	94.6
14	4	0.50	800	0	2.4	8.4	10.2	26.5	27.3	51.1	52.4	70.8	75.5	85.0	88.4
15	5.2	0.32	760	0	3.3	8.9	9.4	25.8	23.3	49.6	46.4	67.7	69.9	87.4	83.7
16	2.8	0.32	640	8.9	6.6	16.6	17.0	39.5	37.0	67.6	63.1	87.6	83.1	96.7	92.1
17	4	0.50	700	8.5	6.8	15.3	16.2	34.0	35.1	60.5	61.1	83.6	82.8	93.5	94.6
18	5.2	0.32	640	4.3	5.2	10.6	12.6	29.3	28.8	54.5	53.4	76.6	76.1	89.6	88.7
19	5.2	0.68	760	2.0	0	10.3	8.4	28.9	26.2	55.3	51.3	74.6	73.2	87.9	85.9
20	2.8	0.32	760	5.1	7.1	12.5	15.8	35.1	33.5	61.5	58.5	80.7	79.6	91.2	90.2

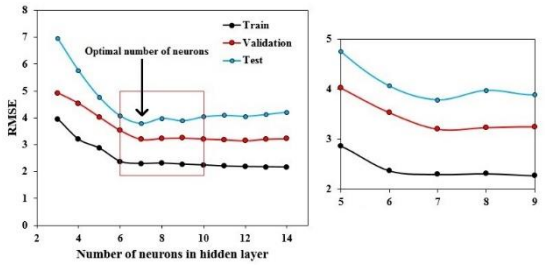

Fig. 8. RMSE versus the number of neurons in the hidden layer for various data sets

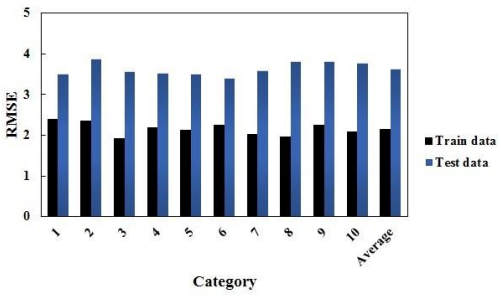

Fig. 9. RMSE values for each selected fold in 10 fold cross-validation method for optimal networks

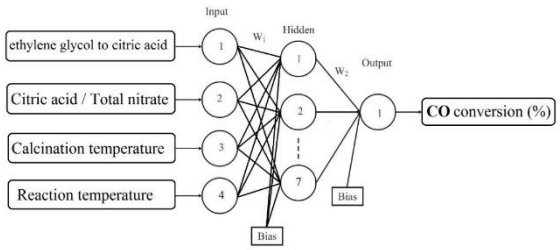

Fig. 10. Schematic of optimum neural network topology

Figure 11 shows the predicted CO conversion results versus experimental data for all datasets. With the perfect fit indicated by the solid line, results in Figure 11 show the good correlative capability of the artificial neural network model. In this prediction, the root means the square error is 2.29, 3.20, and 3.78 for the training, validation, and test data respectively. Besides, the correlation coefficient (R^2) is 0.9948, 0.9920, and 0.9868 for the training, validation, and test data, respectively. The error distribution for CO conversion is shown in Figure 12. The maximum error for CO Conversion is 7.94. It is possible to understand

from Figure 12 that about 87% of all data has errors between -4 and 4, which proves the modeling and prediction ability of gained ANN model.

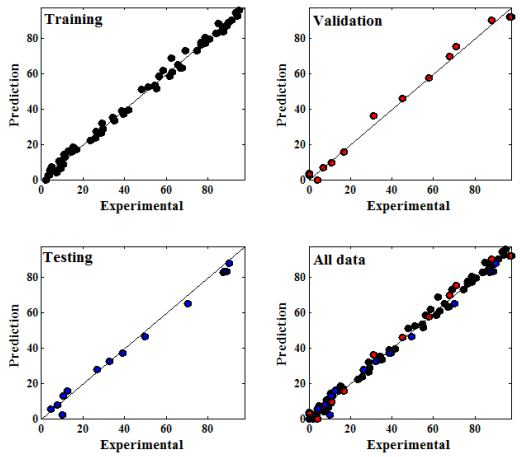

Fig. 11. Comparison between ANN predicted and experimental data

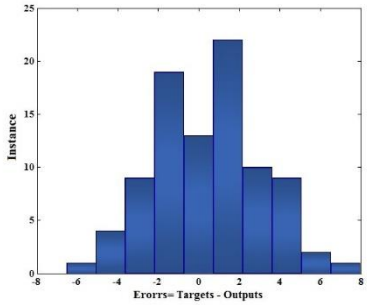

Fig. 12. Error histogram for predicted data with 10 bins

5.3. *Effects of catalyst design variables*

Input parameters analysis was performed to determine the relative importance of CO conversion design parameters. The ANN model analysis was undertaken by equation 7. Figure 13 shows the significance of each parameter relative to others. The results of the analysis show the relative importance of parameters in the conversion of CO. Nevertheless, besides of synthesis parameters, calcination temperature and the ratio of ethylene glycol to citric acid were found to pose the highest and lowest effects onto the output parameter, respectively.

To study the effect of composition and preparation conditions on the performance of catalysts, CO conversion was plotted versus each preparation parameter while other parameters were kept constant. Figure 14a shows the variations in CO conversion versus the citrate/nitrate ratio. This figure indicates the catalyst exhibits high activity when EG/citric acid approaches 3.2. Figure 14b shows the variations in CO conversion versus citric acid to total nitrate. Figure shows, when the citric acid to total nitrate ratio approached 0.6, Catalytic activity increases. Regarding Figure 14c, the highest conversion was observed at 600 to 650 °C. At lower calcination temperatures, increased specific surface area caused improvements in spinel performance.

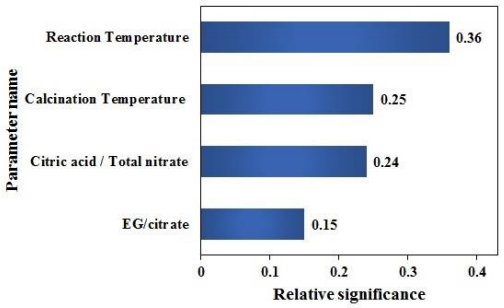

Fig. 13. Relative significance of input variable on CO conversion

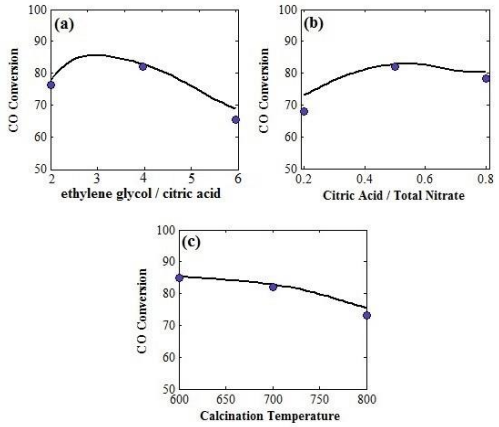

Fig. 14. CO conversion versus catalyst design parameters. In each plot, other variables were fixed at the central point of experimental design, (●) experimental, (-) predicted

5.4. *Optimization of catalyst design variables*

The optimal condition for $CuCr_2O_4$ was predicted by the genetic algorithm. Table 4 indicates the values of different variables in the optimal catalyst. Testing the optimized catalyst shows the experimental results were reasonably close to the predicted values, further confirming the adequacy of the ANN model. Figure 15 shows a comparison between corresponding experimental data and predicted results to the optimum catalyst.

Table 4

Condition for optimal catalyst predicted by the GA method

parameter		value
Catalyst design parameter	EG/CA	3.24
	CA/TN	0.62
	Tcal (°C)	620
CO conversion (%)	Predicted	93.8
	Experimental	92.9

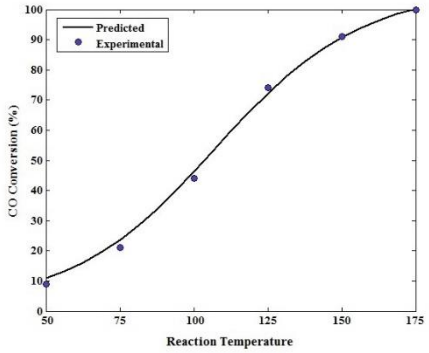

Fig. 15. The temperature profile of CO conversion for optimal catalyst, (●) experimental, (-) predicted

6. Catalyst stability

The stability of $CuCr_2O_4$ catalysts was investigated at 150 °C for 20 h. According to Figure 16, Changes in conversion percentage versus time are not seen. The catalyst showed strong stability in CO oxidation. After 20 h, CO conversions was 82%. The reusability of catalyst was investigated for 5 times. In each experiment, the catalyst was used at 150 °C for 2 h and then cooled for 22 h. This experiment repeated 5 times and the results were shown in Figure 17. The catalyst activity was not changed in this series of experiments.

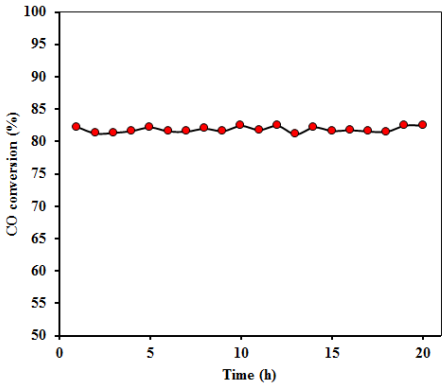

Fig. 16. Stability of $CuCr_2O_4$ catalysts at 150 °C

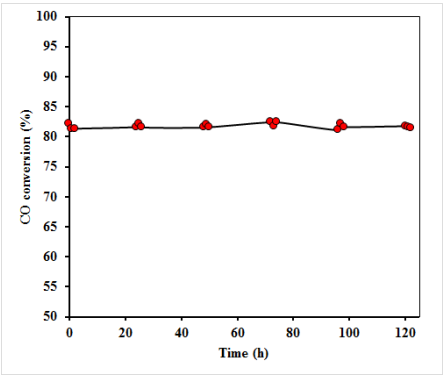

Fig. 17. Reusability of $CuCr_2O_4$ catalysts at 150 °C

7. Conclusions

In this study, an effort was made to model and optimize the catalytic of $CuCr_2O_4$ spinel catalyst in catalytic oxidation of CO using a hybrid ANN-GA approach. Spinel catalysts were prepared by the Pechini method. Selected main factors were EG/citric acid, the ratio of citric acid to total nitrate, calcination temperature (°C), and reaction temperature. A feed-forward back propagation neural network was used to model the relationship between catalytic activity and selected catalyst's design parameters. A good agreement was found between the experimental data and modeling results. The correlation coefficient (R2) was 0.9948, 0.9920, and 0.9868 for the training, validation, and test data. The sensitivity analysis results indicated the calcination temperature as the most significant parameter contributing to the catalyst activity. GA was applied to optimize the catalyst synthesis parameters. Catalyst optimization has increased the CO conversion from 82% in base catalyst to 93% in optimum catalysts. A verification experiment was also performed under the predicted optimum conditions (EG/citric acid: 3.24, citric acid/total nitrate: 0.62 and calcination temperature: 620 °C), and the experimental data (92.9%) was in agreement with the predicted value (93.8%), that indicating the suitability of the model employed and the success of GA in the optimization of synthesis parameters of $CuCr_2O_4$ for catalytic oxidation of CO.

8. Conflicts of interest

There are no conflicts to declare.

9. References

[1] M. Grünbacher, A. Tarjomannejad, P.D.K. Nezhad, C. Praty, K. Ploner, A. Mohammadi, A. Niaei, B. Klötzer, S. Schwarz, J. Bernardi, Promotion of La $(Cu_{0.7}Mn_{0.3})_{0.98}M_{0.02}O_{3-\delta}$ (M= Pd, Pt, Ru and Rh) perovskite catalysts by noble metals for the reduction of NO by CO, Journal of Catalysis 379 (2019) 18-32.

[2] S. Ladas, H. Poppa, M. Boudart, The adsorption and catalytic oxidation of carbon monoxide on evaporated palladium particles, Surface Science 102(1) (1981) 151-171.

[3] X. Tang, J. Hao, J. Li, Complete oxidation of methane on Co_3O_4-SnO_2 catalysts, Frontiers of Environmental Science & Engineering in China 3(3) (2009) 265-270.

[4] L.G. Tejuca, J.L.G. Fierro, J.M. Tascón, Structure and reactivity of perovskite-type oxides, Advances in catalysis, Elsevier1989, pp. 237-328.

[5] R. Voorhoeve, D. Johnson, J. Remeika, P. Gallagher, Perovskite oxides: materials science in catalysis, Science 195(4281) (1977) 827-833.

[6] U.G. Singh, J. Li, J.W. Bennett, A.M. Rappe, R. Seshadri, S.L. Scott, A Pd-doped perovskite catalyst, $BaCe_{1-x}Pd_xO_{3-\delta}$, for CO oxidation, Journal of Catalysis 249(2) (2007) 349-358.

[7] M. Pena, J. Fierro, Chemical structures and performance of perovskite oxides, Chemical reviews 101(7) (2001) 1981-2018.

[8] M. Tomatis, H.-H. Xu, J. He, X.-D. Zhang, Recent development of catalysts for removal of volatile organic compounds in flue gas by combustion: a review, Journal of Chemistry 2016 (2016).

[9] S.C. Kim, The catalytic oxidation of aromatic hydrocarbons over supported metal oxide, Journal of hazardous materials 91(1-3) (2002) 285-299.

[10] J. Kirchnerova, D. Klvana, Design criteria for high-temperature combustion catalysts, Catalysis letters 67(2-4) (2000) 175-181.

[11] P. Stefanov, I. Avramova, D. Stoichev, N. Radic, B. Grbic, T. Marinova, Characterization and catalytic activity of Cu–Co spinel thin films catalysts, Applied surface science 245(1-4) (2005) 65-72.

[12] D. Fino, N. Russo, G. Saracco, V. Specchia, CNG engines exhaust gas treatment via Pd-Spinel-type-oxide catalysts, Catalysis today 117(4) (2006) 559-563.

[13] S. Hosseini, A. Niaei, D. Salari, S. Nabavi, Nanocrystalline AMn_2O_4 (A= Co, Ni, Cu) spinels for remediation of volatile organic compounds—synthesis, characterization and catalytic performance, Ceramics International 38(2) (2012) 1655-1661.

[14] D. Fino, N. Russo, G. Saracco, V. Specchia, Catalytic removal of NOx and diesel soot over nanostructured spinel-type oxides, Journal of Catalysis 242(1) (2006) 38-47.

[15] H. El-Shobaky, Surface and catalytic properties of Co, Ni and Cu binary oxide systems, Applied Catalysis A: General 278(1) (2004) 1-9.

[16] W. Li, W. Chu, M. Zhuang, J. Hua, Catalytic oxidation of toluene on Mn–containing mixed oxides prepared in reverse microemulsions, Catalysis Today 93 (2004) 205-209.

[17] V. Santos, M. Pereira, J. Órfão, J. Figueiredo, The role of lattice oxygen on the activity of manganese oxides towards the oxidation of volatile organic compounds, Applied Catalysis B: Environmental 99(1-2) (2010) 353-363.

[18] L. Markov, A. Lyubchova, Precursor control of the inversion degree of magnesium-cobalt spinels, Journal of materials science letters 10(9) (1991) 512-514.

[19] J.B. Smith, T. Norby, Cation self-diffusion in $LaFeO_3$ measured by the solid state reaction method, Solid State Ionics 177(7-8) (2006) 639-646.

[20] M.E. Günay, R. Yıldırım, Neural network aided design of Pt-Co-Ce/Al_2O_3 catalyst for selective CO oxidation in hydrogen-rich streams, Chemical Engineering Journal 140(1-3) (2008) 324-331.

[21] Z.-Y. Hou, Q. Dai, X.-Q. Wu, G.-T. Chen, Artificial neural network aided design of catalyst for propane ammoxidation, Applied Catalysis A: General 161(1-2) (1997) 183-190.

[22] K. Huang, X.-L. Zhan, F.-Q. Chen, D.-W. Lü, Catalyst design for methane oxidative coupling by using artificial neural network and hybrid genetic algorithm, Chemical Engineering Science 58(1) (2003) 81-87.

[23] M. Munir, M. Saeed, M. Ahmad, A. Waseem, S. Sultana, M. Zafar, G.R. Srinivasan, Optimization of novel Lepidium perfoliatum Linn. Biodiesel using zirconium-modified montmorillonite clay catalyst, Energy Sources, Part A: Recovery, Utilization, and Environmental Effects (2019) 1-16.

[24] K. Huang, F.-Q. Chen, D.-W. Lü, Artificial neural network-aided design of a multi-component catalyst for methane oxidative coupling, Applied Catalysis A: General 219(1-2) (2001) 61-68.

[25] S. Valero, E. Argente, V. Botti, J.M. Serra, P. Serna, M. Moliner, A. Corma, DoE framework for catalyst development based on soft computing techniques, Computers & Chemical Engineering 33(1) (2009) 225-238.

[26] P.R. Zonouz, A. Niaei, A. Tarjomannejad, Modeling and optimization of toluene oxidation over perovskite-type nanocatalysts using a hybrid artificial neural network-genetic algorithm method, Journal of the Taiwan Institute of Chemical Engineers 65 (2016) 276-285.

[27] H. Soleimanzadeh, A. Niaei, D. Salari, A. Tarjomannejad, S. Penner, M. Grünbacher, S.A. Hosseini, S.M. Mousavi, Modeling and optimization of V_2O_5/TiO_2 nanocatalysts for NH3-Selective catalytic reduction (SCR) of NOx by RSM and ANN techniques, Journal of environmental management 238 (2019) 360-367.

[28] R. Haghbakhsh, H. Adib, P. Keshavarz, M. Koolivand, S. Keshtkari, Development of an artificial neural network model for the prediction of hydrocarbon density at high-pressure, high-temperature conditions, Thermochimica acta 551 (2013) 124-130.

[29] P. Saxena, J.C. Patel, M.H. Joshipura, Prediction of vapor pressure of fatty acid methyl esters, Procedia Engineering 51 (2013) 403-408.

[30] R. Eslamloueyan, M. Khademi, Estimation of thermal conductivity of pure gases by using

artificial neural networks, International Journal of Thermal Sciences 48(6) (2009) 1094-1101.
[31] A. Tarjomannejad, Prediction of the liquid vapor pressure using the artificial neural network-group contribution method, Iranian Journal of Chemistry and Chemical Engineering (IJCCE) 34(4) (2015) 97-111.
[32] B. Hameeda, A. Mushtaq, M. Saeed, A. Munir, U. Jabeen, A. Waseem, Development of Cu-doped NiO nanoscale material as efficient photocatalyst for visible light dye degradation, Toxin Reviews (2020) 1-11.
[33] U. Zavyalova, B. Nigrovski, K. Pollok, F. Langenhorst, B. Müller, P. Scholz, B. Ondruschka, Gel-combustion synthesis of nanocrystalline spinel catalysts for VOCs elimination, Applied Catalysis B: Environmental 83(3-4) (2008) 221-228.
[34] A. Salker, S. Gurav, Electronic and catalytic studies on $Co_{1-x}Cu_xMn_2O_4$ for CO oxidation, Journal of materials science 35(18) (2000) 4713-4719.
[35] M. Wojciechowska, M. Zieliński, A. Malczewska, W. Przystajko, M. Pietrowski, Copper–cobalt oxide catalysts supported on MgF2 or Al_2O_3—their structure and catalytic performance, Applied Catalysis A: General 298 (2006) 225-231.
[36] T. Mega, K. Takao, J.-i. Shimomura, State analysis of electrolytic chromate film by XPS and SXS, Applied surface science 121 (1997) 120-124.
[37] B. Grzybowska, J. Słoczyński, R. Grabowski, K. Wcisło, A. Kozłowska, J. Stoch, J. Zieliński, Chromium oxide/alumina catalysts in oxidative dehydrogenation of isobutane, Journal of Catalysis 178(2) (1998) 687-700.
[38] Y. Zhang, W. Xu, J. Zhao, Synthesis of phenylacetonitrile by amination of styrene oxide catalyzed by a bimetallic catalyst $Zn_{30.1}Cr_{4.3}/\gamma$-Al_2O_3, RSC Advances 2(16) (2012) 6590-6598.
[39] M. Saeed, M. Munir, M. Nafees, S.S.A. Shah, H. Ullah, A. Waseem, Synthesis, characterization and applications of silylation based grafted bentonites for the removal of Sudan dyes: Isothermal, kinetic and thermodynamic studies, Microporous and Mesoporous Materials 291 (2020) 109697.